Q. J. R. Meteorol. Soc. (2003), **129**, pp. 2867–2878 doi: 10.1256/qj.02.66

On the time variability of the net ocean-to-atmosphere heat flux in midlatitudes, with application to the North Atlantic basin

By ARNAUD CZAJA*

Massachusetts Institute of Technology, Department of Earth, Atmosphere and Planetary Sciences, Cambridge, USA

(Received 19 February 2002; revised 1 April 2003)

SUMMARY

A new diagnostic to investigate the role of ocean dynamics in midlatitude air–sea interactions is presented and tested against observations. It is based on the analysis of the time variability of the net ocean-to-atmosphere heat flux (F_S).

A hierarchy of air–sea interaction models indicate that, in the absence of ocean dynamics, the power spectrum of F_S should be blue at time-scales longer than a threshold set by the late-winter ocean mixed-layer thickness and the sensitivity of F_S to sea surface temperature anomalies. Comparison of the predicted F_S spectrum with observations over the North Atlantic shows a good agreement over the subpolar gyre where the deep ocean mixed layer combined with strong stochastic forcing allows large fluctuations in F_S at decadal and longer time-scales. Discrepancies, however, arise over the Gulf Stream extension region. Here it is suggested that the observed variability of F_S at time-scales longer than a decade is controlled by geostrophic ocean dynamics rather than local atmospheric forcing.

The diagnostic appears to be a useful and simple tool to investigate the role of ocean dynamics in the upper-ocean heat budget. It is particularly well suited to the analysis of long simulations of coupled ocean–atmosphere models.

One implication of the study for ocean-only numerical simulations is that one cannot specify externally the low-frequency variability of F_S. The latter should only arise as a consequence of ocean dynamics.

KEYWORDS: Air–sea interactions Climate variability North Atlantic Oscillation

1. INTRODUCTION

The net ocean-to-atmosphere heat flux F_S is the sum of turbulent (latent and sensible) and radiative components

$$F_S = F_{turb} + F_{rad}. \tag{1}$$

In midlatitudes, atmospheric variability creates large-scale patterns of anomalous heat flux through its impact on both F_{turb} and F_{rad}. During the cold season, changes in surface wind speed and anomalous cold/warm advection associated with the dominant patterns of atmospheric variability lead to a strong modulation of the turbulent heat flux F_{turb} over the northern hemisphere (e.g. Cayan 1992; Alexander and Scott 1997). During the warm season, changes in cloudiness associated with the anomalous displacement of the storm tracks impact on the radiative component of the heat flux F_{rad} (e.g. Frankignoul 1985; Norris 2000). Thus, the variability of F_S is controlled to a large extent by the variability of atmospheric circulation.

It should be remembered, however, that the net ocean-to-atmosphere heat flux arises solely as a response to a thermodynamic imbalance between the ocean and the atmosphere. In a purely one-dimensional (vertical) framework, without a role for ocean dynamics, the adjustment of the upper ocean to atmospheric variability will lead to an equilibrium state with vanishing net heating/cooling at the surface. Thus, it is expected that at some time-scale the variability of F_S is significantly reduced (blue power spectrum) even though atmospheric state variables (like temperature, pressure) have an essentially white spectrum, or might even be 'reddened' by the interaction with

* Corresponding author: Massachusetts Institute of Technology, Department of Earth, Atmosphere and Planetary Sciences, 77 Massachusetts Avenue, Cambridge, MA 02138, USA. e-mail: czaja@ocean.mit.edu

the ocean. This has been seen in a variety of coupled models that *do not incorporate ocean currents*: energy balance models (Barsugli and Battisti 1998), atmospheric general-circulation models (GCMs) coupled to a slab ocean mixed layer (Bladé 1997).

Ocean dynamics could conceivably sustain a thermodynamic imbalance between the upper ocean and the atmosphere and introduce power in F_S spectra at long time-scales. If, for example, cooling of the upper ocean driven by atmospheric variability through air–sea heat fluxes, is balanced by a warming due to oceanic advection, the variability in net surface heat flux F_S could be enhanced by ocean advection which 'pulls away' the sea surface temperature (SST) anomaly from its thermodynamic equilibrium value. This is seen for instance in the simple coupled model of Saravanan and McWilliams (1998) when oceanic advection becomes sufficiently large compared with damping effects.

It thus appears that a signature of the absence of an impact of ocean dynamics on the upper-ocean heat budget is a weak variability of F_S above a certain time-scale (blue spectrum), which we will refer as τ_o. To our knowledge, this signature, if present in the literature (see the above discussion), has not been discussed and tested against observational datasets. It is the purpose of this paper to determine what sets the time-scale τ_o, and to assess how far one can go in interpreting observations of F_S variability with a model of air–sea interaction which does not include a dynamical ocean. The paper is structured as follows. A model for the variability of F_S is presented in section 2. It is then compared with observations in section 3. Conclusions are offered in section 4.

2. A MODEL FOR THE VARIABILITY OF THE NET OCEAN-TO-ATMOSPHERE HEAT FLUX IN THE ABSENCE OF OCEAN DYNAMICS

(*a*) *A zero-order model*

As a starting point, let us assume that the atmosphere interacts with a slab ocean of constant thickness h_o. In the absence of ocean dynamics, only cooling or warming of the slab can balance fluctuations in the net ocean-to-atmosphere heat flux F'_S (positive upward)

$$\rho C_p h_o \frac{dT'_m}{dt} = -F'_S \tag{2}$$

where ρ and C_p denote the density and specific heat of sea water, respectively, primes indicate deviations from the mean climatological seasonal cycle, and T'_m is the SST anomaly. Let us further decompose F'_S as the sum of an SST-dependent part $\gamma T'_m$ and an independent part N', thus

$$F'_S = -(N' - \gamma T'_m). \tag{3}$$

The N' component reflects that, in midlatitudes, a large fraction of the variability in atmospheric temperature, specific humidity, cloud cover and wind speed exists independently of SST anomalies. It is physically associated with intrinsic dynamical processes within the atmosphere, like baroclinic instability or wave-mean flow interactions. In the absence of further ocean–atmosphere interactions, a simple representation of these processes is to take N' as a stochastic process with a short (a week or so) decorrelation time-scale (Frankignoul and Hasselman 1977; Frankignoul 1985). On the time-scales of interest here (interannual and longer), N' is thus assumed to be a white-noise forcing.

It must be emphasized that despite the assumption of white-noise N', it is not assumed that atmospheric variability, *once coupled with the ocean*, is white. An atmospheric state variable like temperature or geopotential-height anomaly Z' is conceivably

modelled according to $Z' = aN' + fT'_{\mathrm{m}}$ where a is a scaling factor and f measures a dynamical SST feedback on the atmosphere. Depending on the strength of f, atmospheric spectra will depart more or less strongly from that of N (e.g. Barsugli and Battisti 1998; Ferreira *et al.* 2001). For instance, the slight redness hinted at in some observed indices of the North Atlantic Oscillation (NAO) is actually consistent with that expected from a weak interaction with the ocean (Czaja *et al.* 2003).

Combining Eqs. (2) and (3), one sees that the heat-flux sensitivity γ controls the rate of damping of SST anomalies. The precise value of γ depends upon the degree of adjustment of the atmosphere to the SST anomaly. In other words, the parameters γ and f are actually closely related: the larger the feedback f, the weaker the sensitivity γ, because the larger the adjustment of the atmosphere to a given SST anomaly. Were there no adjustment, bulk formulae would lead to a strong sensitivity, $\gamma \simeq 40$ W m^{-2}K^{-1} and strong damping of SST anomalies (Haney 1971; Frankignoul *et al.* 1998). The atmospheric adjustment to SST anomalies reduces this value somewhat, typically by a factor of about 2 in midlatitudes (Frankignoul *et al.* 1998; Czaja *et al.* 2003). Empirical estimates of γ from observations can be found in Frankignoul *et al.* (1998) and Frankignoul and Kestenare (2002), with typical values around 20 W m^{-2}K^{-1}.

Equations (2) and (3) provide a prediction for the power spectrum of F'_{S}

$$|F_{\mathrm{S}}|^2 = \frac{\omega^2}{\omega^2 + {\tau_{\mathrm{o}}}^{-2}} |N|^2 \tag{4}$$

where $|N|^2$ is the power spectrum of the stochastic forcing, ω denotes angular frequency and τ_{o} is a time-scale for the SST anomaly,

$$\tau_{\mathrm{o}} = \frac{\rho C_p h_{\mathrm{o}}}{\gamma}. \tag{5}$$

The separation time-scale τ_{o} depends solely upon the thickness h_{o} of the ocean layer and the heat-flux sensitivity to the SST anomaly γ. For a mixed-layer depth $h_{\mathrm{o}} = 100$ m and sensitivity $\gamma = 20$ W m^{-2}K^{-1}, this amounts to $\tau_{\mathrm{o}} \simeq 8$ months.

Equation (4) indicates that the energy level of $|F_{\mathrm{S}}|^2$ is set by the stochastic forcing $|N|^2$ at high angular frequencies ($\omega \gg {\tau_{\mathrm{o}}}^{-1}$) but behaves like $(\omega\tau_{\mathrm{o}})^2$ at angular frequencies much lower than ${\tau_{\mathrm{o}}}^{-1}$. The power spectrum of the net ocean-to-atmosphere heat flux is thus expected to be blue at periods longer than $2\pi\tau_{\mathrm{o}}$. Figure 1 plots power spectra for different time-scales $\tau_{\mathrm{o}} = 0.25$ years, $\tau_{\mathrm{o}} = 1$ year, $\tau_{\mathrm{o}} = 5$ years and $\tau_{\mathrm{o}} = 10$ years. For a given sensitivity γ and level of stochastic forcing $|N|^2$, if the mixed layer is shallow (small τ_{o}) we see only a weak variability in F_{S} at decadal time-scales, whereas if the mixed layer is deep (large τ_{o}) we observe high-amplitude fluctuations on monthly to decadal time-scales. Conversely, for a given mixed-layer depth h_{o} and level of stochastic forcing $|N|^2$, the larger the adjustment of the atmosphere to SST (i.e. the smaller γ and the larger τ_{o}), the larger the amplitude of the power spectrum of F_{S} at low frequency.

(*b*) *Effects of entrainment and the seasonal cycle*

Some clarifications are needed before comparing the prediction of Eq. (4) with observations. The oceanic mixed-layer depth undergoes a pronounced seasonal cycle in mid- to high latitudes. For instance, over the westerly belt region in the North Atlantic (see below), the late-winter mixed layer typically reaches 500 m, while being only about 25 m in summer (Levitus and Boyer 1994). We thus need to be more specific about the depth used in the above predictions. In addition, the mixed-layer depth also varies from

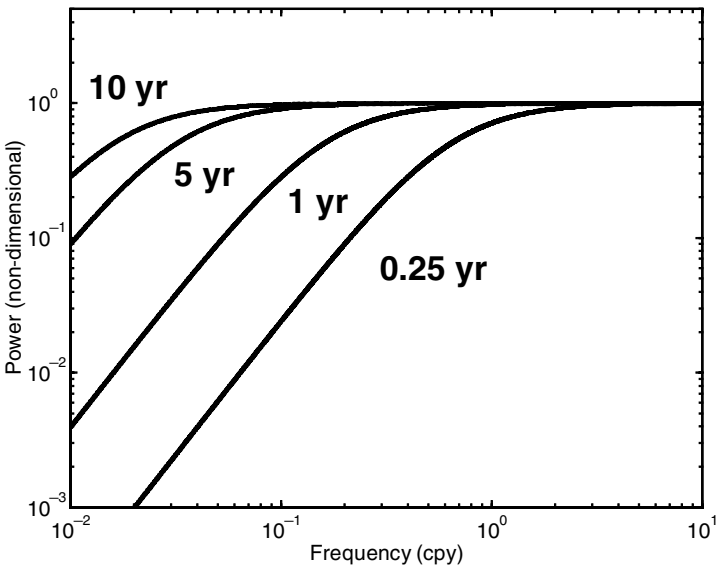

Figure 1. Model prediction for the power spectrum of the net ocean-to-atmosphere heat flux for various time-scales τ_o, as indicated on the plot, and a given level of stochastic forcing. The power is non-dimensional and the frequency is expressed in cycles per year (cpy).

year to year and the associated change in entrainment could complicate the balance of Eq. (2).

Consider first the effects of the climatological mean seasonal cycle. We assume that the ocean mixed-layer thickness h varies seasonally from its shallowest climatological value h_s to its deepest h_d, usually reached in summer and late winter, respectively. At depths above $-h$, the temperature is T_m (the SST), while in between $-h_d$ and $-h$ lies the seasonal thermocline. At depths below $-h_d$ (within the permanent thermocline), the temperature is assumed to be constant. The heat budget can then be written:

$$\frac{\partial}{\partial t}\int_{-h_d}^{0} \rho C_p T' \, dz = -F'_S \tag{6}$$

where T' is the temperature anomaly. Averaging in time from a given late winter (at time $t = t_d$ when $h = h_d$) to the next ($t_d + t_{yr}$, where t_{yr} denotes a year), we have

$$\rho C_p h_d \{T'_m(t_d + t_{yr}) - T'_m(t_d)\} = -\int_{t_d}^{t_d+t_{yr}} F'_S \, dt \tag{7}$$

since $T'(t_d) = T'_m(t_d)$ and $T'(t_d + t_{yr}) = T'_m(t_d + t_{yr})$. Equation (7) thus suggests that the annually averaged anomaly in F_S is related to the model Eq. (2) with the mixed-layer thickness set to its deepest climatological value ($h_o = h_d$), and the annual average estimated from one late winter to the next.

A similar dependence of annually averaged conditions upon late-winter mixed-layer depth was recently demonstrated by Deser *et al.* (2003) (see also de Coëtlogon and Frankignoul 2003) when considering extratropical SST anomalies. Note, however, that their argument about re-emergence (memory of SST anomalies from late winter to the following early winter due to entrainment at the base of the seasonally varying ocean mixed layer) is not part of the argument presented here, although re-emergence is present

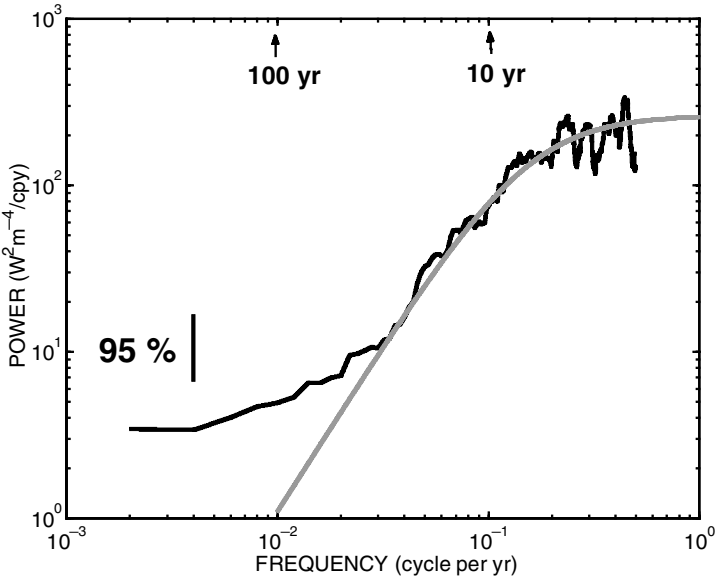

Figure 2. Power spectrum of annually averaged net surface heat-flux anomalies simulated by Alexander and Penland (1996) at 50°N–145°W (black curve) and that predicted by the simple model of section 2(a) (grey curve). The frequency is expressed in cycles per year (cpy), and the power in W^2m^{-4}/cpy, as computed using the multitaper method (Percival and Walden 1993). The vertical line indicates a 95% confidence level.

in the above conceptual model (temperature anomalies in the seasonal thermocline are those generated the previous winter). Equation (7) is merely an annual average of the mixed-layer heat budget, not an annual average of the various processes governing the damping of SST anomalies through the course of a year.

To test that the model Eq. (2) should indeed be used with $h_o = h_d$ and the annual average estimated from one late winter to the next, and further to assess how entrainment effects impact on the simple prediction of Eq. (4), we now turn to a long simulation (500 years) of a state-of-the-art ocean mixed-layer model driven by stochastic atmospheric forcing. The simulation is described in detail in Alexander and Penland (1996). It is sufficient to note here that anomalous fields of wind speed, air temperature and specific humidity were derived from different Markov models and added to a seasonally varying climatology to force the ocean mixed-layer model of Gaspar (1988). The latter includes a sophisticated parametrization of entrainment at the bottom of the mixed layer and a diffusive thermocline below the mixed layer.

We compare the simulated and predicted spectra in Fig. 2. Annually averaged F_S anomalies were first computed for the simulation by starting from the time of the deepest mixed layer (t_d) which, for the simulation, coincides with January (i.e. the annual average is from January to January). The power spectrum of the annual anomalies was then estimated (black curve). The predicted spectra (grey curve) was constructed from Eq. (4), using $h_o = h_d = 120$ m and $\gamma = 15$ W $m^{-2}K^{-1}$, which was estimated from the monthly cross-covariance function of SST and net surface heat-flux anomalies, as described in Frankignoul *et al.* (1998). The stochastic-forcing energy level $|N|^2$ was set to that of the simulated spectrum at high frequency (using an average of the monthly spectrum over the frequency band 1–3 cycles per year (cpy), i.e. periods between 4 months and 1 year, outside of the frequency range shown in Fig. 2). One observes a good agreement between the two spectra on interannual to interdecadal time-scales.

The simulated spectrum is blue, with a spectral slope close to +2 for time-scales ranging from about 5 to 30 years. This suggests a short time-scale τ_0 (see Fig. 1), consistent with our estimate $\tau_o \simeq 1$ year (using $h_d = 120$ m and $\gamma = 15$ W m^{-2}K^{-1}—see Eq. (5)). The model Eq. (4), however, fails to predict the flattening of the spectrum on longer time-scales (centuries). This probably reflects the effects of vertical diffusion which, on these long time-scales, act to increase the thickness of the oceanic layer interacting with the atmosphere.

In summary, despite the reddening of atmospheric state-variable spectra created by the interaction of the atmosphere with a motionless ocean (e.g. Barsugli and Battisti 1998), the absence of ocean dynamics prevents such low-frequency (decadal and longer) fluctuations existing for F_S, unless, (i) the atmosphere interacts with a very deep ocean mixed layer or (ii) the atmosphere adjusts so strongly to SST anomalies that it reduces the sensitivity of the net heat flux, γ, to values close to zero. We now discuss the form of observed spectra of F_S and compare them with our simple model.

3. Comparison with observations

We focus on two specific regions of the North Atlantic, the westerly belt (60–15°W, 45–60°N, hereafter WB) and the Gulf Stream extension (80–40°W, 25–45°N, hereafter GS). This choice is motivated by the relatively good data coverage over these areas, and their different oceanic conditions, such as late-winter mixed-layer depth. This should allow us to test the model of section 2 in different parameter regimes. In addition, as shown in various studies (e.g. Cayan 1992; Marshall *et al.* 2001), changes in wintertime surface cooling of the ocean in these regions is known to be associated with changes in the North Atlantic Oscillation (NAO), the dominant signal of interannual variability of the northern-hemisphere atmosphere. This makes these regions of particular relevance to climate variability over the North Atlantic.

A major issue in comparing the prediction of Eq. (4) with observed F_S spectra is the significant error expected in the estimation of F_S from either atmospheric re-analyses or *in situ* oceanographic observations. To take this explicitly into account in the comparison, we rewrite Eq. (4) as

$$|F_S|^2 = \frac{\omega^2}{\omega^2 + \tau_o{}^{-2}}|N|^2 + n^2|N|^2 \tag{8}$$

where n is a parameter measuring the uncertainty we allow in the surface heat flux. It is assumed that observational errors are uncorrelated with the true estimate of the surface heat flux and can be represented as white noise with amplitude proportional to $|N|^2$. For instance, a value $n = 0.5$ postulates a 50% error in F_S. The impact of the error term in Eq. (8) will be small at high frequencies but can significantly alter (and 'whiten') the low-frequency part of the blue shape spectrum as n gets closer to unity (see below). In the following we will consider $n = 1$ and $n = 0$, the truth being somewhere between perfect data and a 100% error.

To apply the prediction of Eq. (8), we further need to estimate the time-scale τ_o and the energy level of stochastic forcing $|N|^2$. In accordance with the previous section, we set h_o to the late-winter mixed-layer depth h_d ($h_d = 500$ m for WB and $h_d = 120$ m for GS) observed by Levitus and Boyer (1994). The sensitivity γ is roughly known from observations (see section 2(a)) but we decided to produce a prediction for weak and strong sensitivities, expecting typical F_S spectra to fall in between those curves. In Figs. 3 (WB) and 4 (GS) these two predictions define an envelope shown as a dashed

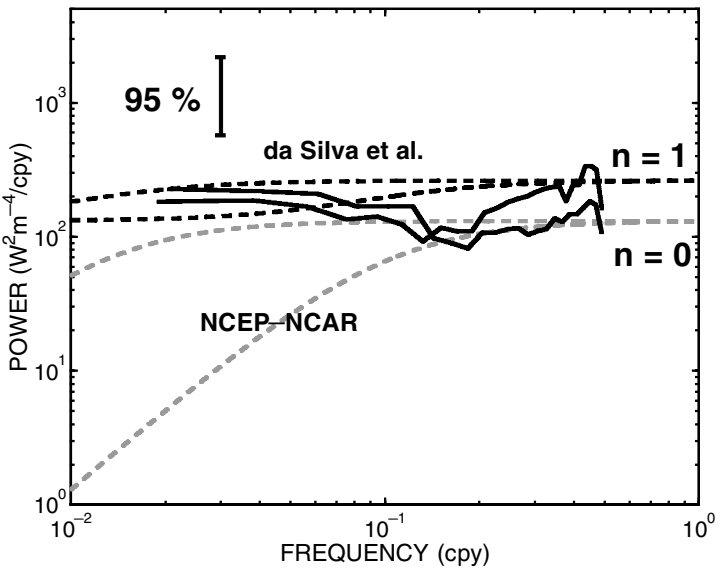

Figure 3. As in Fig. 2, but for the power spectrum of observed annually averaged (and linearly detrended) anomalies in net ocean-to-atmosphere heat flux F_S over the westerly belt region (from National Centers for Environmental Prediction (NCEP)/National Center for Atmospheric Research (NCAR) re-analysis over 1949–2001 and da Silva *et al.* (1994) over 1945–93, continuous curves) and the prediction of the simple model for different sets of parameters (dashed curves). An approximate error bar for the observed spectra is indicated on the upper left corner.

line, two envelopes being shown, one for $n = 1$ (100% error in F_S, black) and the other for $n = 0$ (perfect data, grey). For each envelope, the lowest curve corresponds to the strongest sensitivity (set to 40 W m^{-2}K^{-1}, with a shorter τ_o), while the uppermost curve corresponds to the weakest sensitivity (set to 5 W m^{-2}K^{-1}, with a longer τ_o).

To estimate the level of stochastic forcing $|N|^2$ we have averaged the spectrum of observed monthly F_S anomalies over the frequency band 1–3 cpy, as in Fig. 2. This was done separately using F_S from the National Centers for Environmental Prediction (NCEP)/National Center for Atmospheric Research (NCAR) re-analysis (Kalnay *et al.* 1996) and from da Silva *et al.* (1994). We then averaged the two estimates to estimate $|N|^2$. The spectrum of both the NCEP/NCAR and the da Silva surface heat flux are shown in Figs. 3 and 4 as continuous black curves*.

Comparison of the observed spectra with the model prediction (either $n = 0$ or $n = 1$) over the WB region (Fig. 3) indicates no major discrepancy, the observed spectrum being within error bars (indicated on the upper left corner of Fig. 3) of the prediction envelopes. The deep mixed layer in that region leads to a white spectrum for the theoretical prediction over a broad range of frequencies for high and low sensitivities γ ($n = 0$, grey envelope), this being even more pronounced when including large errors in F_S ($n = 1$, black envelope). Thus, for this region, the observed, essentially white net heat-flux spectrum merely reflects atmospheric variability interacting with a deep ocean mixed layer. This interpretation is further reinforced by the comparison of the

* To maintain consistency with section 2, annually averaged anomalies were first computed as averages from February (March) to the following February (March) for the WB (GS) region ($t = t_d$ of section 2(b)), based on the seasonal climatology of mixed-layer depth from Levitus and Boyer (1994). However, the results turned out to be insensitive to this choice and calendar annual averaging is used in the following analysis.

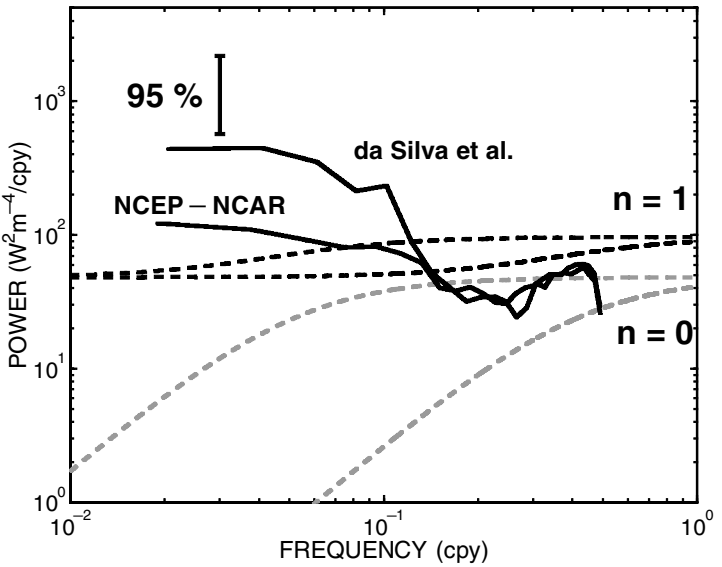

Figure 4. As in Fig. 3, but for the Gulf Stream extension region.

time series of F_S over the WB region with Hurrell's NAO index (Hurrell 1995), which varies in phase from interannual to interdecadal time-scales (not shown).

More severe departures from the model prediction, however, occur for the Gulf Stream extension region (Fig. 4). If observed and predicted spectra (perfect case, $n = 0$, grey envelope) agree within error bars out to decadal periods, the low-frequency end of the observed spectra (either NCEP/NCAR or da Silva) is significantly higher than that predicted for both large or weak sensitivities (more than one order of magnitude departure at time-scales longer than 25 years). Taking into account observational errors suggests that, in the worst case ($n = 1$, black envelope), we should expect a white spectrum even though the mixed layer is sufficiently shallow to, in principle, lead to a blue spectrum (grey envelope), were ocean dynamics actually negligible. However, both NCEP/NCAR and da Silva estimates are still above this limit, suggesting a slightly red power spectrum for the observed F_S over the Gulf Stream extension region. In other words, the late-winter mixed-layer depth is too shallow for local atmospheric forcing alone to account for the observed amplitude of F_S anomalies at low frequencies.

As perhaps the simplest possible mechanism by which ocean dynamics might improve the model of section 2 over the GS region, we study the role of anomalous Ekman advection F'_{Ek} by modifying Eq. (2) as,

$$\rho C_p h_o \frac{dT'_m}{dt} = -F'_S - F'_{Ek} \tag{9}$$

with

$$F'_{Ek} \equiv \rho C_p \left(U'_{Ek} \frac{\partial \bar{T}_m}{\partial x} + V'_{Ek} \frac{\partial \bar{T}_m}{\partial y} \right) \tag{10}$$

and where $\bar{T}_m$ is the climatological mean SST and (U'_{Ek}, V'_{Ek}) is the anomalous Ekman mass transport (simply a function of latitude and the anomalous wind-stress vector). As far as the surface heat flux is concerned, the essential modification introduced by the inclusion of Ekman processes is a possible balance between Ekman advection

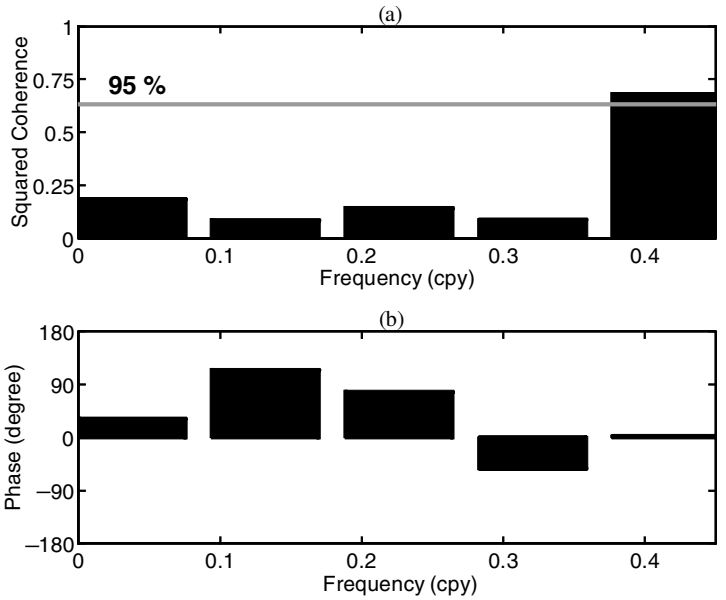

Figure 5. (a) Squared coherence and (b) phase (in degrees) between annually averaged anomalies of net surface heat flux (F'_S) and Ekman heat advection (F'_{Ek}), averaged over the Gulf Stream extension region. F'_{Ek} was first computed from Eq. (10) for each month using monthly wind-stress anomalies, and the climatological mean sea-surface-temperature seasonal cycle from the National Centers for Environmental Prediction (NCEP)/National Center for Atmospheric Research (NCAR) re-analysis, then annually averaged. The co-spectrum was averaged over five frequency bins (expressed in cycles per year, cpy), with a 95% confidence level indicated for the squared coherence as the horizontal line.

and surface heating/cooling on time-scales when the storage term becomes small, i.e. typically τ_o (a few years). This balance ($F'_{Ek} \simeq -F'_S$) might, if F'_{Ek} is sufficiently large, result in larger-amplitude F_S anomalies at decadal and longer time-scales than accounted for by the model of section 2 and so enhance the power of F_S at low frequency.

To check this, we have computed the spectral coherence between F'_S and an estimate of F'_{Ek}, both constructed from the NCEP/NCAR re-analysis (Fig. 5). One sees that it is only at the highest frequencies (periods of about 2 years) that a significant coherence is found, with very small coherence at lower frequencies (Fig. 5(a)). This is a first indication that the balance $F'_{Ek} \simeq -F'_S$ does not occur at low frequencies. In addition, the phase difference between F'_{Ek} and F'_S is close to zero for most of the frequency bins rather than being close to ± 180 degrees (Fig. 5(b)). This reflects that anomalous surface easterlies reduce wind speed and hence turbulent heat fluxes over the GS region, while simultaneously creating an anomalous northward Ekman current. Both act together to warm the upper ocean rather than oppose each other as the balance requires. Finally, F'_{Ek} is typically found to be a factor of about 2 to 3 times smaller than F'_S at interannual time-scales, with a power spectrum almost one order of magnitude lower than that of F_S at time-scales of decades or longer (not shown).

It thus appears very unlikely that anomalous Ekman currents alone could be responsible for the discrepancy between predicted and observed slow changes in F'_S over the GS region, which points to a role for geostrophic ocean dynamics in that region. Overall, our conclusions are consistent with modelling studies of SST variability (e.g. Battisti *et al.* 1995; Halliwell 1998; Seager *et al.* 2000). Halliwell (1998) for

example showed that over the westerly belt region geostrophic ocean dynamics are not needed to simulate the basic structure of interdecadal SST variability, whereas it is crucial in the Gulf Stream extension region.

4. Conclusions

A prediction for the power spectrum of the net ocean-to-atmosphere heat flux was derived from a simple stochastic model of air–sea interaction, and tested in more elaborate models and observations over the North Atlantic ocean. In the absence of ocean dynamics, the spectrum is predicted to show a characteristic time-scale τ_o, above which the spectrum is blue (power decreasing with time-scale) and below which it is white (power nearly constant with time-scale). The time-scale τ_o is set by the late-winter mixed-layer depth h_d and the sensitivity of the net heat flux to SST change γ.

Predicted and observed surface heat-flux spectra are in agreement over the subpolar gyre of the North Atlantic (60–15°W, 45–60°N, or westerly belt region WB). In that region of deep late-winter mixed-layer depth ($h_d = 500$ m), the time-scale τ_o is sufficiently large that, as observed, the predicted spectrum is white from interannual to interdecadal time-scales. Thus, over that region, one-dimensional air–sea interactions alone are able to create pronounced decadal and longer time-scale fluctuations in surface heat flux.

The situation is more complicated over the Gulf Stream extension region (80–40°W, 25–45°N, or GS), however, where the late-winter mixed-layer depth reaches only 120 m. For both large and weak sensitivity γ, the associated time-scale τ_o is too short to account for the slight redness displayed by the observed spectrum. Thus, over the Gulf Stream extension region, one-dimensional air–sea interaction is not sufficient to explain low-frequency fluctuations in surface heat flux. Geostrophic dynamics are thus postulated to be involved in driving SST away from a thermodynamic equilibrium with the atmosphere, thereby allowing the observed changes in surface heat flux at decadal and longer time-scales.

It is suggested that analysis of the low-frequency variability of F_S provides a robust way to diagnose the impact of ocean dynamics on the upper-ocean heat budget, particularly in regions of relatively shallow ocean mixed layers. The impact of ocean currents on SST typically represents a modulation, of about a factor of 2 or 3, of its canonical red power spectrum in certain frequency bands (e.g. Czaja and Marshall 2001). It is of about one order of magnitude for F_S (going from a blue to a white or red spectrum), which makes the ocean-dynamics signature easier to detect.

Although the diagnostic presented here could easily be applied to oceanic regions other than the North Atlantic basin, uncertainties in observed F_S datasets make the diagnostic even more relevant to coupled ocean–atmosphere numerical models. It allows a simple and straightforward alternative (h_d is easily diagnosed from the model temperature profile, γ is easily estimated from the covariance between SST and F_S anomalies—see Frankignoul *et al.* (1998)) to the explicit computation of each term of the mixed-layer heat budget. Of course, the latter will still be needed to identify the physical mechanisms (horizontal or vertical advection) responsible for the enhanced power of F_S at low frequency.

One implication of this study is that one cannot specify externally the time behaviour of F_S in forced ocean-only numerical simulations. The atmospheric control of F_S variability was shown to be limited by the finite heat capacity of the ocean mixed layer and the non-zero sensitivity of F_S to SST anomalies. The presence of significant power in F_S spectra at time-scales of decades or longer must reflect the impact of ocean dynamics on the mixed-layer heat budget. This impact can easily be included by adding

an SST-dependent term to any prescribed low frequency for F_S (as in Eq. (3)), keeping in mind that it implicitly makes an assumption about the atmospheric adjustment to SST anomalies.

Whether the small changes in the heat flux observed at interdecadal time-scales over the Gulf Stream extension region (peak-to-peak amplitude of about 10 W m^{-2}) and attributed to ocean dynamics in this study could significantly impact on the atmospheric circulation deserves further study.

ACKNOWLEDGEMENTS

Mike Alexander kindly provided model outputs of F_S. Discussions with C. Wunsch are gratefully acknowledged. This work was supported by a grant from the National Oceanographic and Atmospheric Administration's Office of Global Programs as part of Atlantic CLImate VARiability (CLIVAR).

REFERENCES

Alexander, M. A. and Penland, C. 1996 Variability in a mixed layer ocean model driven by stochastic atmospheric forcing. *J. Climate*, **9,** 2424–2442

Alexander, M. A. and Scott, J. D. 1997 Surface flux variability over the North Pacific and North Atlantic oceans. *J. Climate*, **10,** 2963–2978

Barsugli, J. J. and Battisti, D. S. 1998 The basic effects of atmosphere–ocean thermal coupling on midlatitude variability. *J. Atmos. Sci.*, **55,** 477–493

Battisti, D. S., Bhatt, U. S. and Alexander, M. A. 1995 A modeling study of the interannual variability of the North Atlantic Ocean. *J. Climate*, **8,** 3067–3083

Bladé, I. 1997 The influence of midlatitude ocean–atmosphere coupling on the low-frequency variability in a GCM: 1. No tropical SST forcing. *J. Climate*, **10,** 2087–2106

Cayan, D. 1992 Latent and sensible heat flux anomalies over the northern oceans: Driving the sea surface temperature. *J. Phys. Oceanogr.*, **22,** 859–881

Czaja, A. and Marshall, J. 2001 Observations of atmosphere–ocean coupling in the North Atlantic. *Q. J. R. Meteorol. Soc.*, **127,** 1893–1916

Czaja, A., Robertson, A. W. and Huck, T. 2003 'The role of coupled processes in producing NAO variability'. Pp. 147–172 in Geophysical Monograph 134, AGU

Da Silva, A. M., Young, C. G. and Levitus, S. 1994 *Atlas of surface marine data, vol 1: Algorithms and procedures.* NOAA Atlas NESDIS 6, US Department of Commerce, Washington DC, USA

De Coëtlogon, G. and Frankignoul, C. 2003 On the persistence of sea surface temperature in the North Atlantic. *J. Climate*, **16,** 1364–1377

Deser, C., Alexander, M. A. and Timlin, M. S. 2003 Understanding the persistence of sea surface temperature anomalies in midlatitudes. *J. Climate*, **16,** 57–72

Ferreira, D., Frankignoul, C. and Marshall, J. 2001 Coupled ocean–atmosphere dynamics in a simple midlatitude climate model. *J. Climate*, **14,** 3704–3723

Frankignoul, C. 1985 Sea surface temperature anomalies, planetary waves and air–sea feedbacks in the middle latitudes. *Rev. Geophys.*, **23,** 357–390

Frankignoul, C. and Hasselman, K. 1977 Stochastic climate models. II: Applications to sea surface temperature variability and thermocline variability. *Tellus*, **29,** 289–305

Frankignoul, C. and Kestenare, E. 2002 The surface heat flux feedback. I: Estimates from observations in the Atlantic and the North Pacific. *Clim. Dyn.*, **19,** 633–647

Frankignoul, C., Czaja, A. and L'Hévéder, B. 1998 Air–sea feedback in the North Atlantic and surface boundary conditions for ocean models. *J. Climate*, **11,** 2310–2324

Gaspar, P. 1988 Modeling the seasonal cycle of the upper ocean. *J. Phys. Oceanogr.*, **18,** 161–180

Halliwell, G. 1998 Simulation of North Atlantic decadal/multidecadal winter SST anomalies driven by basin-scale atmospheric circulation anomalies. *J. Phys. Oceanogr.*, **28,** 5–21

Haney, R. L. 1971 Surface thermal boundary conditions for ocean circulation models. *J. Phys. Oceanogr.*, **1,** 241–248

Hurrell, J. W. 1995 Decadal trends in the North Atlantic Oscillation: Regional temperatures and precipitation. *Science*, **269,** 676–679

Kalnay, E., Kanamitsu, M., Kistler, R., Collins, W., Deaven, D., Gandin, L., Iredell, M., Saha, S., White, G., Woollen, J., Zhu, Y., Chelliah, M., Ebisuzaki, W., Higgins, W., Janowiak, J., Mo, K. C., Ropelewski, C., Wang, J., Leetmaa, A., Reynolds, R., Jenne, R. and Joseph, D. 1996 The NCEP/NCAR 40-year reanalysis project. *Bull. Am. Meteorol. Soc.*, **77**, 437–472

Levitus, S. and Boyer, T. 1994 *World Ocean Atlas, vol 4: Temperature.* NOAA Atlas NESDIS 4, US Department of Commerce, Washington DC, USA

Marshall, J., Johnson, H. and Goodman, J. 2001 A study of the interaction of the North Atlantic Oscillation with the ocean circulation. *J. Climate*, **4,** 1399–1421

Norris, J. R. 2000 Interannual and interdecadal variability in the storm-track, cloudiness, and sea surface temperature over the summertime North Pacific. *J. Climate*, **13,** 422–430

Percival, D. B. and Walden, T. A. 1993 *Spectral analysis for physical applications. Multitaper and conventional univariate techniques.* Cambridge University Press

Saravanan, R. and McWilliams, J. C. 1998 Advective ocean–atmosphere interaction: An analytical stochastic model with implications for decadal variability. *J. Climate*, **11,** 165–188

Seager, R., Kushnir, Y., Visbeck, M., Naik, N., Miller, J., Krahman, G. and Cullen, H. 2000 Causes of Atlantic ocean climate variability between 1958 and 1998. *J. Climate*, **13,** 2845–2862